

Novel Machaeriol Analogues as Modulators of Cannabinoid Receptors: Structure–Activity Relationships of (+)-Hexahydrocannabinoids and Their Isoform Selectivities

Saqlain Haider, Pankaj Pandey, Chada Raji Reddy, Janet A. Lambert, and Amar G. Chittiboyina*

Cite This: *ACS Omega* 2021, 6, 20408–20421

Read Online

ACCESS |



Metrics & More

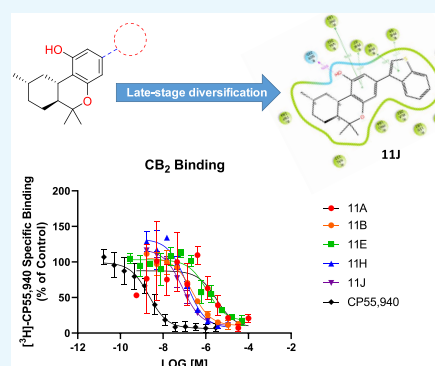


Article Recommendations



Supporting Information

ABSTRACT: Machaeriols are an important class of compounds that structurally resemble tetrahydrocannabinol (Δ^9 -THC), with the major differences being inverted stereochemistry at the ring junction as [6aR, 10aR] and an additional stereocenter at the C9 position of the A-ring due to saturation. A previous study reported that machaeriols did not show any cannabinoid receptor activity, even though these hexahydrodibenzopyran analogues mimic a privileged (+)-tetrahydrocannabinoid scaffold. To unravel structural requisites for modulation of cannabinoid receptors, a simple late-stage divergent approach was undertaken to functionalize the machaeriol scaffold using the Suzuki coupling reaction. Fourteen hexahydro analogues were synthesized and screened against both cannabinoid receptor isoforms, CB₁ and CB₂. Interestingly, many of the analogues showed a significant binding affinity for both receptors; however, two analogues, 11H and 11J, were identified as possessing CB₂ receptor-selective functional activity in the GTP γ S assay; they were found to be micromolar-range agonists, with EC₅₀ values of 5.7 and 16 μ M, respectively. Furthermore, molecular dynamics simulations between the CB₂ receptor and two novel analogues resulted in unique interaction profiles by tightly occupying the active ligand-binding domain of the CB₂ receptor and maintaining stable interactions with the critical residues Phe94, Phe281, and Ser285. For the first time, with the aid of structure–activity relationships of (+)-hexahydrocannabinoids, CB₂ selective agonists were identified with late-stage diversification using palladium-mediated C–C bond formation. By simply switching to (*R*)-citronellal as a chiral precursor, enantiomerically pure (–)-hexahydrocannabinoids with better CB₁/CB₂ receptor isoform selectivity can be obtained using the current synthetic approach.



1. INTRODUCTION

More than 100 natural phytocannabinoids have been isolated and characterized from *Cannabis sativa*; tetrahydrocannabinol (Δ^9 -THC) and cannabidiol (CBD) are the two best-studied phytoconstituents (Figure 1).¹ CB₁R and CB₂R, the cannabinoid receptors, are part of the endocannabinoid system (ECS), which comprises the endogenous ligands and their related enzymes and transporters. CB₁ receptors are expressed in the central nervous system (CNS) and are also found in the body's periphery, including the testes, eyes, vascular endothelium, and spleen,² while CB₂ receptors are found mostly in the immune and gastrointestinal systems.² The expression of the CB₂ receptor in the CNS is very low compared to that of the CB₁ receptor, which makes it an attractive target to avoid possible CNS side effects. Some previously studied therapeutic benefits of CB₂R agonists are analgesic and anti-inflammatory effects.^{3–5} CB₂R agonists have shown efficacy as potential therapeutic agents in peripheral diseases that involve inflammation, such as atherosclerosis,⁶ renal fibrosis,⁷ and liver cirrhosis.⁸ The ECS is involved in many human diseases and may provide potential drug development targets, including fatty acid amide hydrolase, monoacylglyceride lipase, and an anandamide transporter.^{9,10}

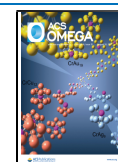
Δ^9 -THC is a partial CB₁ and CB₂ receptor agonist, whereas CBD is a weak antagonist or a negative allosteric modulator (at the CB₁R level) of the CB₁/CB₂ receptor.^{11–13}

The pharmacological activity of Δ^9 -THC is stereospecific, i.e., the (–)-trans-isomer (dronabinol, FDA approved) is 6–100 times more potent than the (+)-trans-isomer.¹⁴ Machaeriols are another important class of structurally similar compounds to THC and were first isolated by Muhammad et al. in 2001 from *Machaerium multiflorum* Spruce.¹⁵ Machaeriols have a hexahydrodibenzopyran scaffold (Figure 1). The structural difference between THC and machaeriols is that the ring junction stereochemistry in machaeriols is inverted with an additional stereocenter at the C9 position in the A-ring; therefore, machaeriols are not tetrahydrocannabinoids but are instead hexahydrocannabinoids. Intrigued by the structural similarity

Received: May 7, 2021

Accepted: July 9, 2021

Published: July 28, 2021



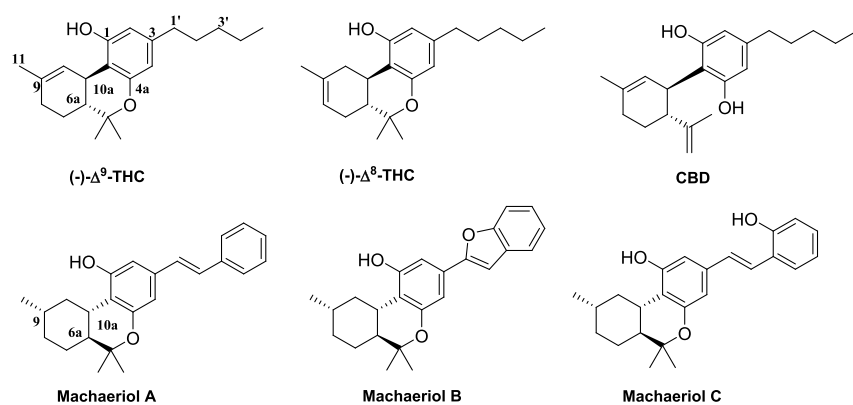
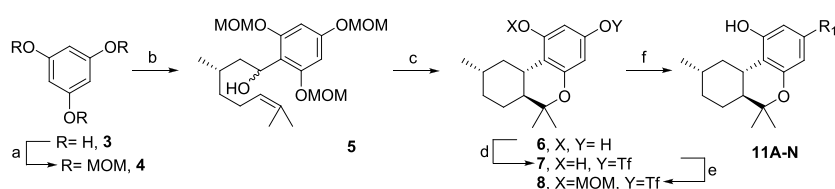


Figure 1. Structural similarity between THC, CBD, and machaeriols.

Scheme 1. Reagents and Conditions^a



^aNaH, MOMCl, THF, 30 min, 95%; (b) *n*-BuLi, TMEDA, 0 °C, (*S*)-citronellal, 30 min, 85%; (c) 4% aqueous HCl in MeOH, rt, 12 h, 65%; (d) PhNTf₂, Et₃N, CH₂Cl₂, 3 h, 74%; (e) NaH, MOMCl, THF, 30 min, 97%; and (f) (1) boronic acid, Pd(PPh₃)₄, 2 M aq Na₂CO₃, MeOH, toluene, reflux, 2 h and (2) 1% aq HCl in MeOH, reflux, 30 min.

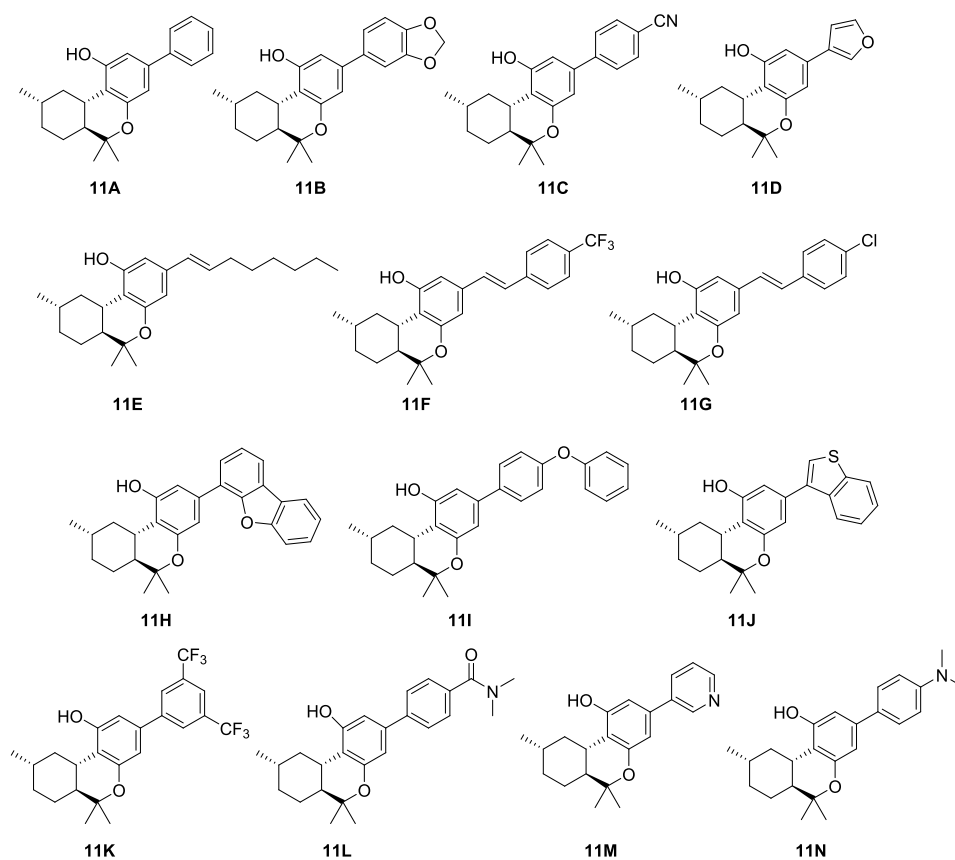


Figure 2. Structures of diverse compounds 11A–11N synthesized using Scheme 1.

between Δ^9 -THC and machaeriols and in continuation of our previous efforts, we report herewith the late-stage diversification of 14 novel derivatives of machaeriol-like analogues from a

common precursor, hexahydrobenzopyran. The cannabimimetic activities of these novel analogues were probed with CB₁ and CB₂ receptors in displacement assays, and their functional

activity was confirmed with GTP γ S assays. We further extended our study to evaluate the putative binding modes and interaction profiles of promising compounds **11J** (against CB₁R and CB₂R) and **11H** (against CB₂R only), using molecular dynamics (MD) simulation and binding free-energy calculations.

2. RESULTS AND DISCUSSION

2.1. Synthesis of Machaeriol Analogues. Continuing our previous synthetic work on the total synthesis of machaeriols A and B, lithiated methoxymethyl (MOM)-protected phloroglucinol was condensed with (*S*)-citronellal (Scheme 1).¹⁶ Mild acid-mediated deprotection of MOM groups induced the intramolecular hetero-Diels–Alder cycloaddition to produce hexahydrodibenzopyran (**6**) in 65% isolated yield with >98% diastereoselectivity. Selective triflation followed by MOM protection of the remaining phenol yielded a key intermediate, **8**, amenable for the late-stage diversification. Palladium (0)-mediated Suzuki coupling of compound **8** with various boronic acids allowed the introduction of several aryl/alkyl moieties at the C3 position of the hexahydrochromane scaffold. Acid-mediated deprotection of the MOM group produced 14 diverse analogues, **11A**–**11N**, with excellent yields (Scheme 1, Figure 2).

2.2. In Vitro Competitive Radioligand Displacement Assays for CB₁ and CB₂ Receptors. In preliminary probing, the synthesized compounds were assayed at a single concentration of 10 μ M for their *in vitro* CB₁ and CB₂ percent displacement. The highly potent and nonselective CB agonist CP55,940 was used as a positive control.¹⁷ The compounds that showed >50% displacement of the radioligand [³H]-CP55,940 at the CB receptors were further assayed over a range of concentrations using a competitive radioligand binding assay to estimate binding affinities (K_i values). Two compounds (**11E** and **11J**) exhibited low micromolar CB₁R displacement, with IC₅₀ values ≤ 1.0 μ M (Figure 3 and Table 1). Among the 14

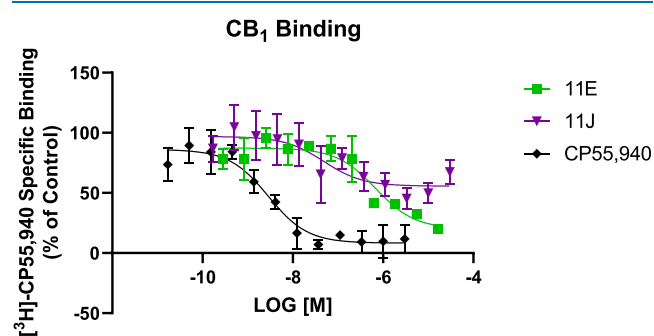


Figure 3. Binding displacement curves for the CB₁ receptor were obtained for compounds **11E** and **11J** with a radioligand binding assay. CP55,940 was used as a positive control. IC₅₀ and K_i were determined by GraphPad Prism 9.1 and are listed in Table 1. The data represent mean \pm SEM. Each compound was tested in triplicate.

compounds evaluated in the competitive radioligand binding assay (Table 1), compounds **11B**, **11H**, and **11J** (Figure 4) showed significant displacement at the CB₂ receptor, yielding binding affinities with IC₅₀ values in submicromolar/high nanomolar levels except for **11A** and **11E** (Figure 4 and Table 1). Compound **11E**, having an octenyl chain at the C3 position similar to CBD and Δ^9 -THC (pentyl chain), exhibited a higher CB₁R binding affinity as compared to other compounds lacking the alkyl chain. The presence of a bulky aromatic substitution at

the C3 position (**11H** and **11J**) resulted in a superior CB₂R binding affinity in comparison with those having small aromatic rings (**11A**, **11C**, **11D**, and **11K**).

2.3. In Vitro GTP γ S Functional Assays for CB₁ and CB₂ Receptors. Using membrane preparations similar to the radioligand binding methods and GTP γ [³⁵S], the functional behavior (e.g., agonists, antagonists, or inverse agonists) of the most promising compounds was determined using GTP γ S functional assays.⁹ Compound **11J** was tested using CB₁ and CB₂ functional assays, while **11H** was tested using the CB₂ functional assay only. All were determined to act as agonists, with the most promising being **11H** (EC₅₀ = 5730 \pm 3289 nM) against the CB₂ receptor. Compound **11J** showed an EC₅₀ value of 1471 \pm 708 nM against the CB₁ receptor, while at the CB₂ receptor, it showed a moderate EC₅₀ value of 15 993 \pm 8631 nM, confirming its preference toward the CB₁ receptor as an agonist (Figures 5 and 6). Compound **11E** was tested using the CB₁ functional assay and was identified as a CB₁R agonist with an EC₅₀ value of 239 \pm 68 nM.

2.4. Molecular Docking Studies. Molecular docking studies were performed to understand the binding pose and orientation of **11E**, **11J**, and **11H** into the active sites of the CB₁ and CB₂ receptor protein crystal structures. Extra precision (XP) docking (Glide, Schrödinger) was used with flexible ligand sampling, keeping the receptor rigid.^{18,19} Compound **11E** exhibited strong π – π stacking interactions, with Phe170 and Phe268, resulting in a GlideScore of –9.79 kcal/mol and a binding free energy (ΔG) of –68.02 kcal/mol. Furthermore, the octenyl chain at the C3 position of **11E** showed strong hydrophobic interactions with an array of residues, Val196, Phe200, Ile267, Leu276, Trp279, Trp356, Leu359, Met363, and Cys386 (Figure 7A,C). Similarly, the hexahydrochromane scaffold and the benzothiophene moiety of compound **11J** exhibited strong π – π stacking interactions with Phe170, Phe268, and Trp279 (Figure 7B,C), resulting in a GlideScore of –9.91 kcal/mol and a binding free energy (ΔG) of –66.39 kcal/mol. This double π – π interaction is reported with a co-crystallized agonist in the active-state X-ray crystal structure (PDB ID: 5XRA) of the CB₁ receptors.¹⁷ The octenyl chain at the C3 position and the benzothiophene moiety of compounds **11E** and **11J**, respectively, were oriented toward the toggle switch residues Phe200 and Trp356. The benzothiophene moiety of **11J** formed π – π stacking with Trp279. The oxygen atom of the benzopyran ring system of **11J** was found to be at a distance of 3.5 Å from the key residue of the CB₁ receptor Ser383,¹⁷ indicating that **11J** can form hydrogen bonding with Ser383, if residue flexibility is permitted. In addition, **11J** showed strong hydrophobic interactions with an array of hydrophobic residues, including Phe108, Phe174, Phe177, Leu193, Val196, Phe200, Ile267, Trp279, Trp356, Leu359, Phe379, Ala380, and Cys386, as shown in Figure 7. Furthermore, we compared the docked pose of Δ^9 -THC with **11E** and **11J** into the active site of the CB₁ receptor and found that they overlaid in a similar fashion and exhibited identical π – π stacking interactions with Phe170 and Phe268. However, **11E** and **11J** did not form H-bonding with Ser383, which was observed in the Δ^9 -THC docked pose. Interestingly, upon close analysis, the ligand-binding orientation of hexahydrochromane **11E** and **11J** was significantly different from that of Δ^9 -THC (Figure 7D). The core scaffold of **11E** and **11J** was horizontally inverted by positioning the hydroxyl group away from the Ser383 residue, which showed the lack of direct H-bonding between **11J** and CB₁.

Table 1. Percent (%) Displacement and Binding Affinity (K_i) of 11A–11N against CB₁ and CB₂ Receptors in Radioactive Competition Assays^a

compound	% displacement at 10 μ M		$K_i \pm$ SEM (nM)		IC ₅₀ \pm SEM (nM)	
	CB ₁	CB ₂	CB ₁	CB ₂	CB ₁	CB ₂
11A	34.33	57.34	nd	1574 \pm 836	nd	3148 \pm 1672
11B	30.77	66.97	nd	117.2 \pm 11.7	nd	2350 \pm 23
11C	-7.02	22.14	nd	nd	nd	nd
11D	34.03	44.40	nd	nd	nd	nd
11E	66.85	50.41	342.0 \pm 95.8	572.8 \pm 105.8	683.9 \pm 325.9	1146 \pm 212
11F	43.21	23.94	nd	nd	nd	nd
11G	7.54	8.70	nd	nd	nd	nd
11H	29.45	76.18	nd	63.68 \pm 8.19	nd	127.4 \pm 16.4
11I	34.37	16.31	nd	nd	nd	nd
11J ^b	56.36	70.40	>1000	40.18 \pm 2.91	>2000	80.35 \pm 5.82
11K	-26.66	11.21	nd	nd	nd	nd
11L	nd	nd	nd	nd	nd	nd
11M	nd	nd	nd	nd	nd	nd
11N	nd	nd	nd	nd	nd	nd
CP55,940	101.12	98.94	1.43 \pm 0.24	1.07 \pm 0.12	2.86 \pm 0.46	2.15 \pm 0.24

^and, not determined. Each compound was tested in triplicate unless stated otherwise. ^bDid not reach baseline.

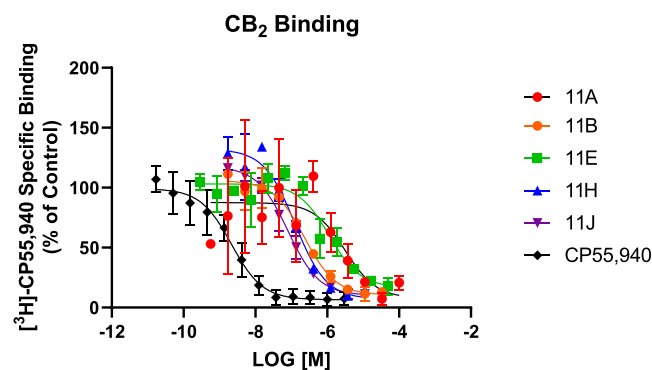


Figure 4. Binding displacement curves for the CB₂ receptor were obtained for compounds 11A, 11B, 11E, 11H, and 11J with a radioligand binding assay. CP55,940 was used as a positive control. IC₅₀ and K_i were determined by GraphPad Prism 9.1 and are listed in Table 1. The data represent mean \pm SEM. Each compound was tested in triplicate.

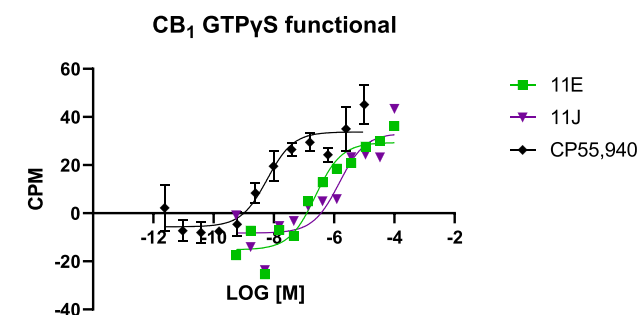


Figure 5. GTP γ S functional curves for compounds 11E and 11J against the CB₁ receptor. EC₅₀ values were determined by GraphPad Prism 9.1. Each compound was tested in duplicate.

In a similar fashion, the docking and binding free-energy data revealed that compounds 11H (GlideScore = -10.80 kcal/mol; ΔG = -64.14 kcal/mol) and 11J (GlideScore = -10.07 kcal/mol; ΔG = -67.64 kcal/mol) bound more tightly and exhibited stronger interactions with the CB₂ receptor. Compounds 11H and 11J were well docked into the active site of the CB₂R cryo-

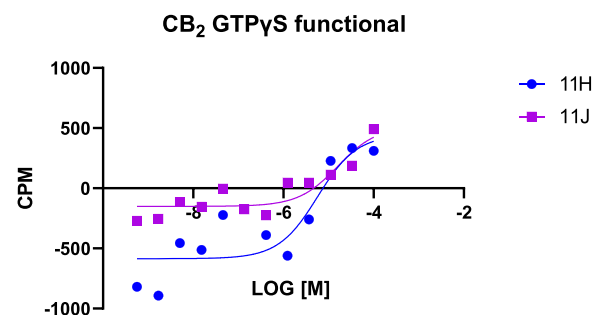


Figure 6. GTP γ S functional curves for compounds 11H and 11J against the CB₂ receptor. EC₅₀ values were determined by GraphPad Prism 9.1. Each compound was tested in duplicate.

EM structure (PDB ID: 6PT0) (Figure 8A,B). The 3D overlaid representation of 11H and 11J against the CB₂ receptor is shown in Figure 8C. The hexahydrochromane moiety of compounds 11H and 11J was oriented toward the toggle-switch residues Phe117 and Trp258. The benzofuran moiety of 11H formed strong π - π stacking interactions with Phe94 and His95. In addition, the hydroxyl group (C1) of compounds 11H and 11J showed H-bonding with Ser285, which is known to be a critical residue for CB₂R activity.²⁰ Furthermore, the benzothiophene and benzopyran rings of compound 11J exhibited π - π stacking interactions with Phe94 and Phe183, respectively. Both compounds 11H and 11J were surrounded by the hydrophobic residues of the CB₂ receptor, including Tyr25, Ile27, Ile110, Phe117, Phe183, Tyr190, Leu191, Trp194, Ile198, Trp258, Val261, Leu262, and Phe281 (Figure 8).

We compared the docked pose of Δ^9 -THC with 11J and 11H against the CB₂ receptor and found that they overlaid well with Δ^9 -THC in the active site of the CB₂ receptor (Figure S1). However, the substituted C3 moieties of 11H and 11J were vertically inverted compared to the C5 alkyl chain of Δ^9 -THC (Figure 8). They also maintained the key interactions of Δ^9 -THC with the CB₂ receptor, including Ser285 (H-bonding) and Phe183 (π - π interactions).

2.5. Molecular Dynamics Simulation Studies. Molecular docking represents a static snapshot of the protein–ligand complex and sometimes may not predict the exact pose of the

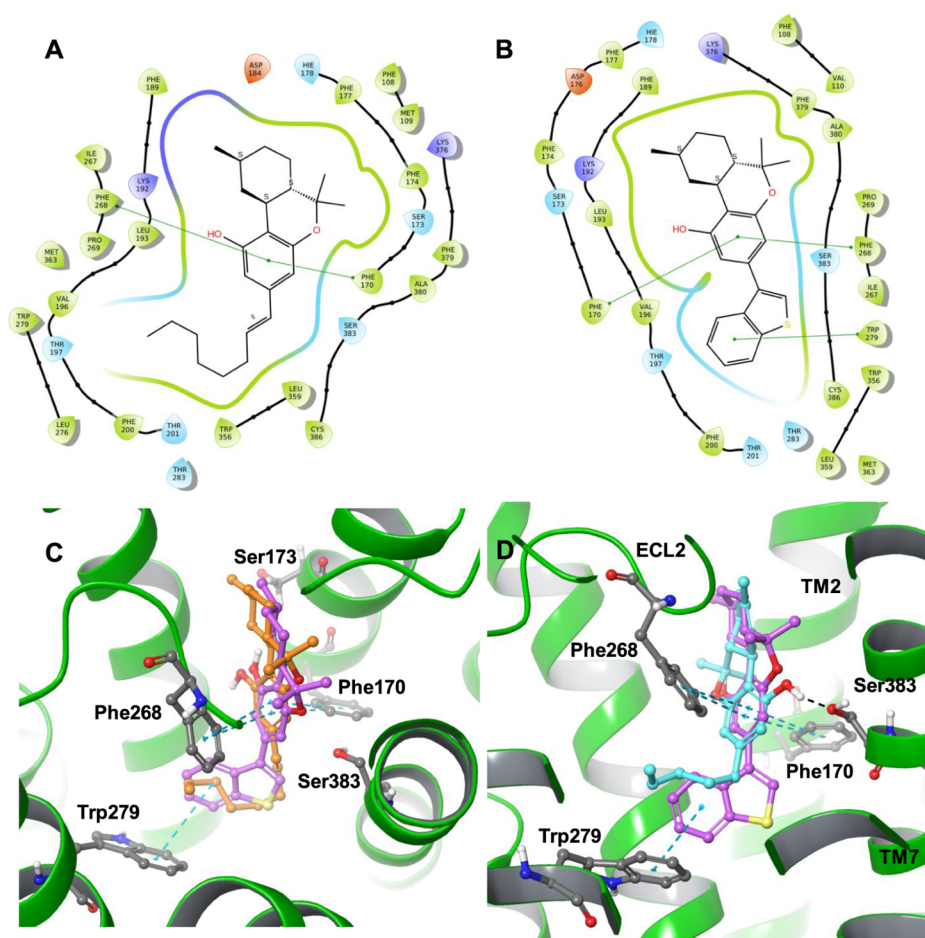


Figure 7. 2D interaction diagrams of 11E (A) and 11J (B) along with the 3D overlaid representation of 11E (carbon in orange) with 11J (carbon in plum) (C) and 11J (carbon in plum) with Δ^9 -THC (carbon in cyan) (D) against the CB₁ receptor. The key residues are shown in the ball and stick model (carbon in gray), and transmembrane regions are shown as ribbons (green-colored).

ligand within the protein active site.^{18,21} Therefore, MD simulation is an excellent technique to further confirm the stability of the protein–ligand complex and study the interaction profiles as it evolves over time. To explore the conformation dynamics of the best-docked complexes of CB₂R–11H, CB₂R–11J, and CB₁R–11J, 200 ns MD simulations were performed. The root-mean-square deviations (RMSDs) of the protein α atoms and ligand heavy atoms were calculated with reference to the starting structures (first frame at time 0 ns) and are shown in Figures 9 and 10. The RMSD of the protein α atoms of CB₂R proteins in the complex of CB₂R–11H and CB₂R–11J varied between 1 and 1.5 Å during the whole simulation, which is an acceptable range for GPCR proteins.¹⁹ Similarly, the RMSD of ligand heavy atoms of

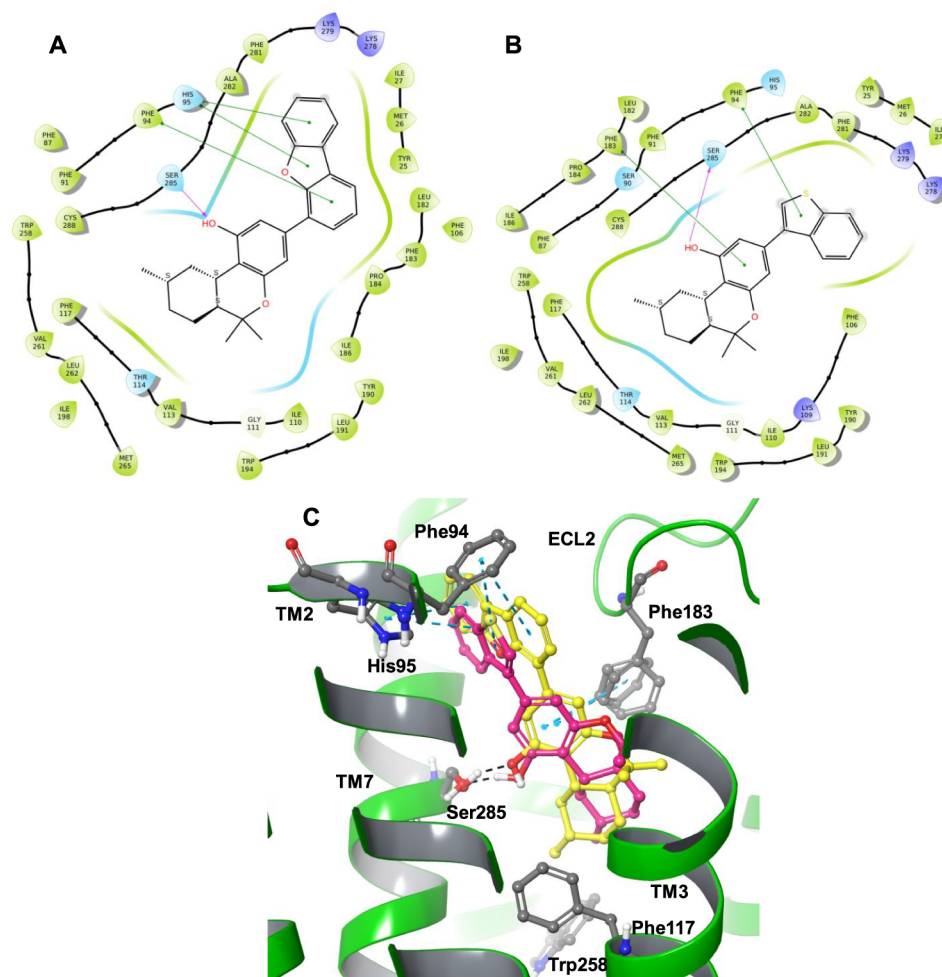


Figure 8. 2D interaction diagrams of 11H (A) and 11J (B) along with the 3D overlaid representation of 11H (carbon in yellow) and 11J (carbon in plum) (C) against the CB₂ receptor. The key residues are shown in the ball and stick model (carbon in gray) and transmembrane regions are shown as ribbons (green-colored).

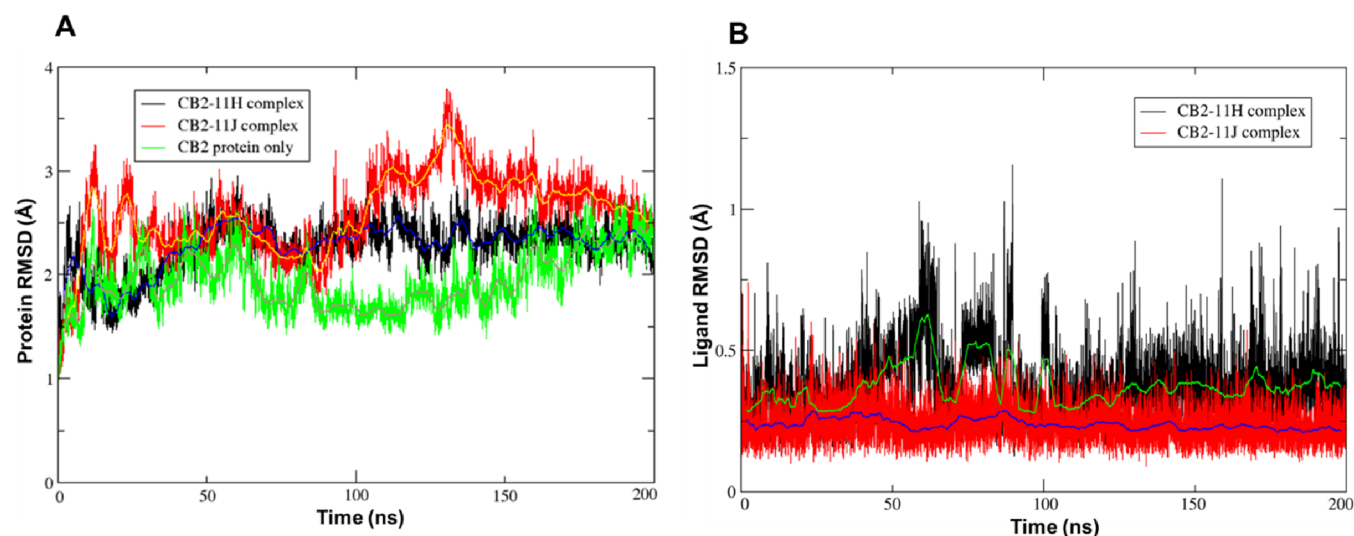


Figure 9. RMSD for the C α atoms of (A) proteins and (B) ligand heavy-atom RMSD for MD simulations of complexes 11H and 11J with the CB₂ receptor.

fluctuation was observed to be <1.4 Å (Figure S3), also supporting the stability of the complex. The interaction histogram (Figure 13) and 2D ligand contact map (Figure 14)

of 11J with the CB₂ receptor indicate a strong H-bonding of the OH of 11J with Ser285 (93% contribution) and π - π stacking with Phe183 (71% contribution), Phe87 (40% contribution),

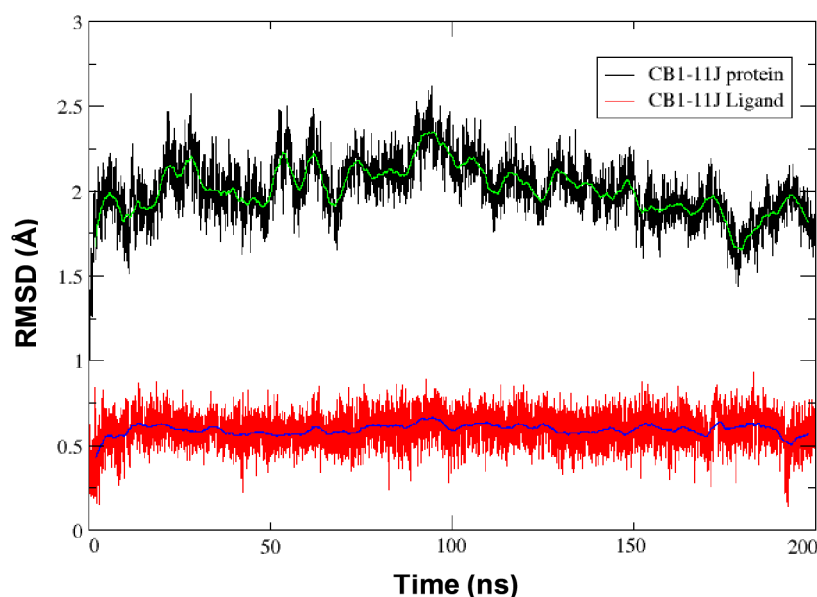


Figure 10. Heavy-atom ligand RMSD for complex 11J with the CB₁ receptor.

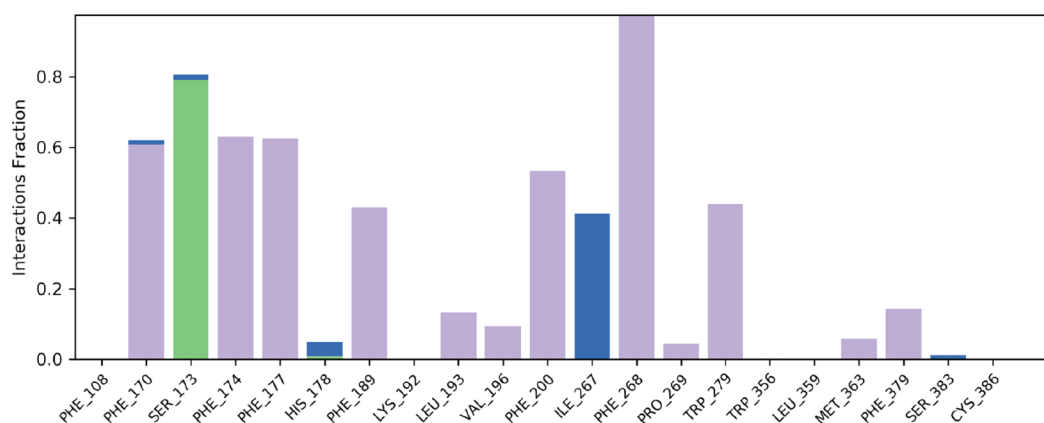


Figure 11. Simulation interaction diagram (SID) plot showing the protein–ligand interactions between the amino acid residues of the CB₁ receptor binding site and 11J. Interaction-fraction values over 1.0 indicate that the residue has multiple contacts with the ligand.

Phe91 (48% contribution), and Phe94 (22% contribution). Interestingly, no water-mediated interaction was observed in the entire simulation of the CB₂R–11J complex. It also shows an array of hydrophobic interactions with the Ile27, Val113, Leu182, Pro184, Trp194, Val261, Phe281, and Ala282. The higher negative average binding free energy ($\Delta G = -81.42 \pm 5.09$ kcal/mol) after the post-MD of 11J with the CB₂ receptor affirmed its complex stability (Table 2). Overall, 11J formed stable and strong interactions with the CB₂ receptor.

2.5.3. CB₂R–11H Complex. The RMSF plot based on the C α atoms of CB₂R for complexes with 11H showed very low fluctuations for the residues that form the ligand-binding site. The overall fluctuation was observed to be <1.3 Å (Figure S4), supporting the stability of the complex. The interaction histogram (Figure 15) and 2D ligand contact map (Figure 16) of 11H with the CB₂ receptor indicate a strong H-bonding of the OH of 11H with Ser285 (85% contribution) and π – π stacking with Phe87 (75% contribution), Phe91 (47% contribution), Phe94 (39% contribution), and Phe183 (73% contribution). Interestingly, similar to 11J, no water-mediated interaction was observed during the entire 200 ns simulation. 11H also exhibited an array of hydrophobic interactions with Ile27, Val113, Leu182,

Pro184, Trp194, Val261, Phe281, and Ala282. The negative average binding free energy ($\Delta G = -91.55 \pm 4.90$ kcal/mol) of 11H after post-MD simulation confirmed the stability of the CB₂–11H complex (Table 2). In summary, strong H-bonding of 11H with Ser285 and multiple π – π stacking with CB₂R residues resulted in a stable complex of CB₂R–11H.

The most negative average binding free energy ($\Delta G = -91.55 \pm 4.90$ kcal/mol) for 11H (CB₂) was contributed by the van der Waals interactions (vdW) (-60.29 ± 2.51 kcal/mol), along with other significant contributions from the Lipo term (a measure of hydrophobic interactions with water) (-39.56 ± 2.17 kcal/mol), π – π stacking interaction (-5.74 ± 1.02 kcal/mol), and Coulombic term (Coulomb) or electrostatic interactions (-11.98 ± 2.14 kcal/mol). Similar trends were observed for 11J (CB₁ and CB₂ receptors). Binding free-energy data of 11J against CB₁ and CB₂ receptors showed correlation with experimental functional data in terms of EC₅₀; however, the receptor binding affinity does not corroborate.

3. CONCLUSIONS

To probe the cannabimimetic activity of (+)-hexahydrocannabinoids, a small set of 14 novel analogues were synthesized

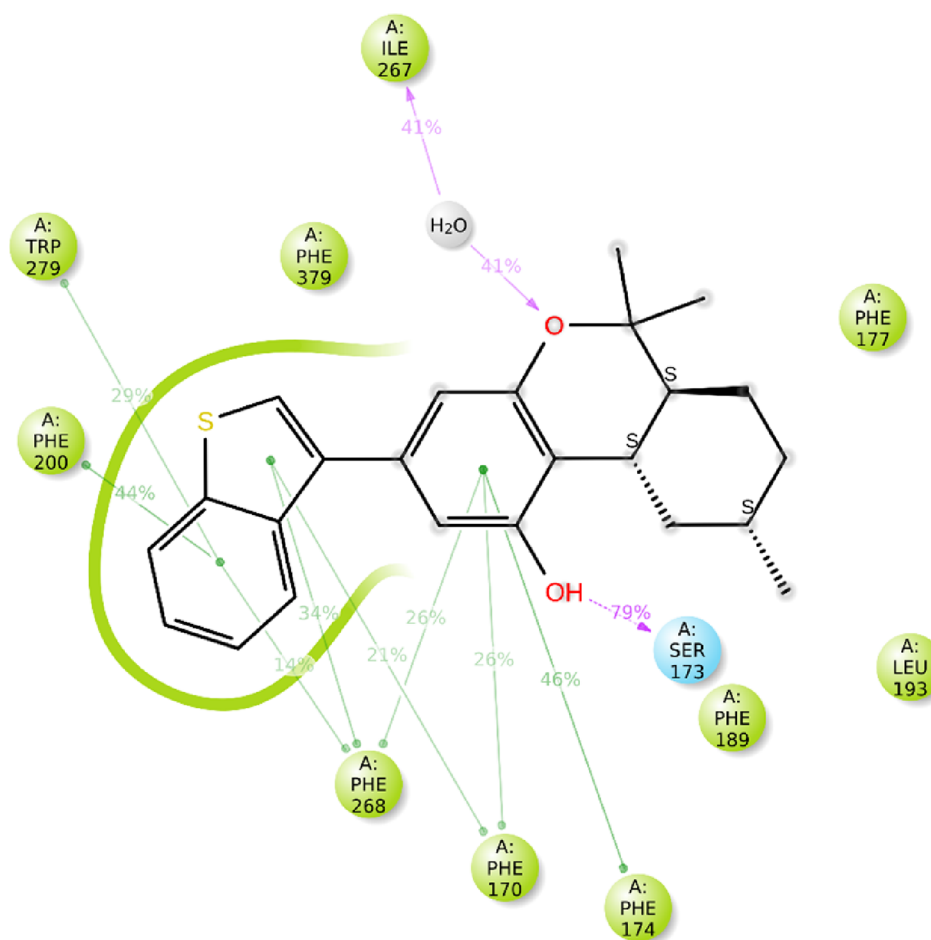


Figure 12. 2D diagram of atomic-level interactions of the CB₁R–11J complex with key CB₁ residues during the 200 ns MD simulation.

Table 2. Prime MM-GBSA Binding Free Energies (Post-MD Simulations) for 11H (CB₂) and 11J (CB₁ and CB₂) Receptors^a

	ΔG average binding free energy (\pm SD)	Coulomb (\pm SD)	covalent (\pm SD)	H-bond (\pm SD)	Lipo (\pm SD)	π -packing energy (\pm SD)	SolvGB (\pm SD)	vdW (\pm SD)
11H (CB ₂)	-91.55 ± 4.90	-11.98 ± 2.14	3.66 ± 1.86	-0.48 ± 0.15	-39.56 ± 2.17	-5.74 ± 1.02	22.85 ± 1.83	-60.29 ± 2.51
11J (CB ₁)	-82.95 ± 4.89	-11.10 ± 2.80	2.31 ± 1.01	-0.42 ± 0.15	-33.96 ± 1.61	-4.77 ± 0.79	23.25 ± 1.63	-58.25 ± 1.83
11J (CB ₂)	-81.42 ± 5.09	-12.74 ± 2.29	2.54 ± 1.09	-0.51 ± 0.10	-32.24 ± 1.80	-4.30 ± 0.69	21.18 ± 1.95	-55.35 ± 2.40

^aCoulomb: Coulomb energy; covalent: covalent binding energy; vdW: van der Waals energy; Lipo: lipophilic energy; SolvGB: generalized Born electrostatic solvation energy; and H-bond: hydrogen-bonding energy.

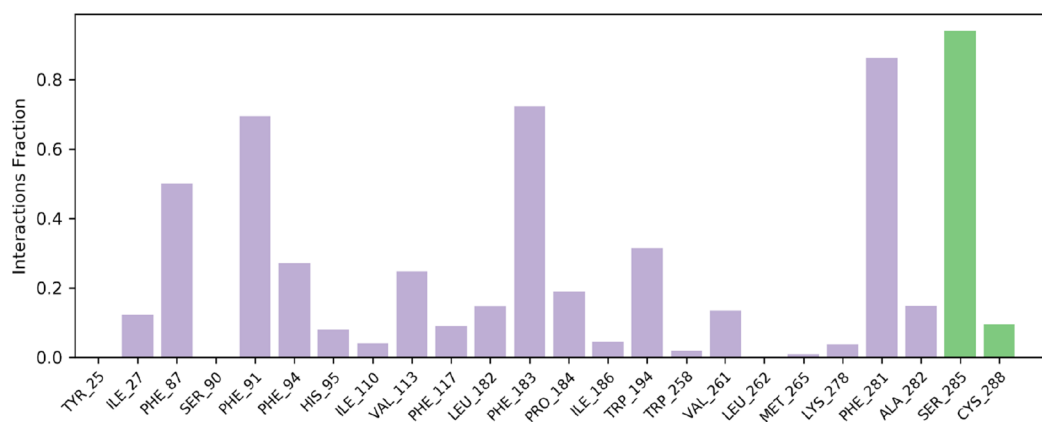


Figure 13. SID plot showing the protein–ligand interactions between the amino acid residues of the CB₂ receptor binding site and 11J.

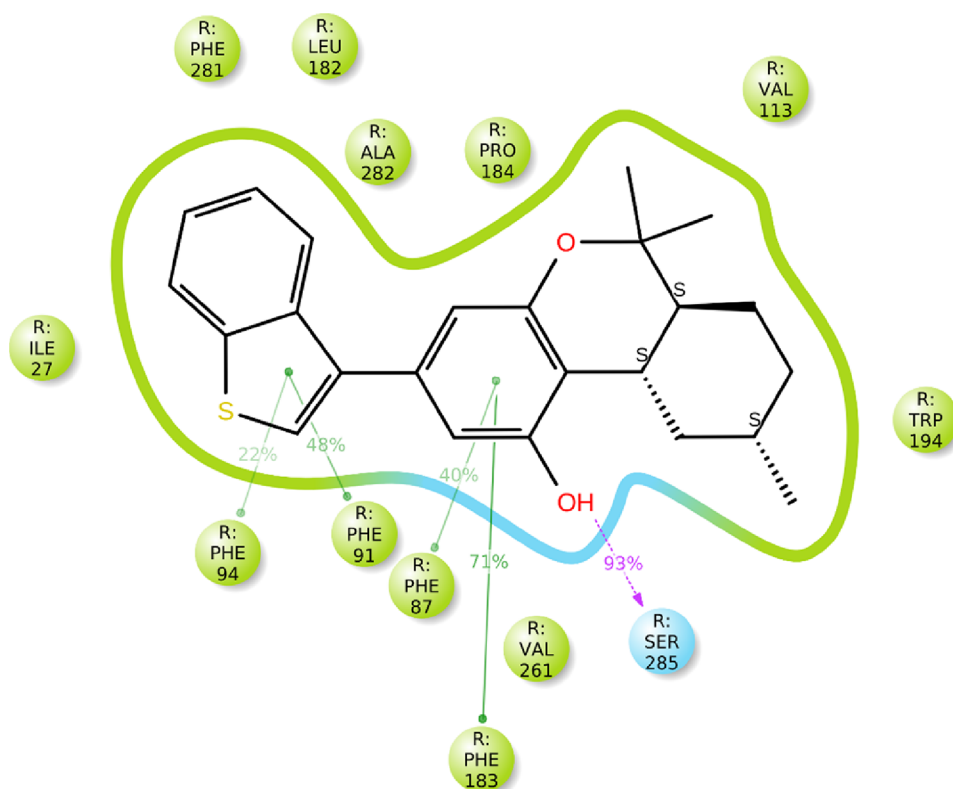


Figure 14. 2D diagram of atomic-level interaction of the CB₂-11J complex with key CB₂R residues during the 200 ns MD simulation.

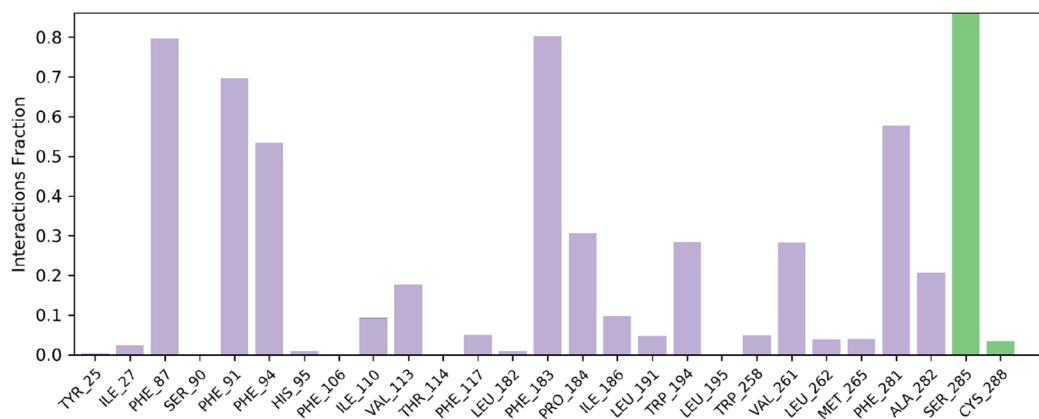


Figure 15. SID plot showing the protein-ligand interactions between the amino acid residues of the CB₂ receptor binding site and 11H.

readily from (*S*)-citronellal using a late-stage diversification approach. These analogues were screened against CB₁ and CB₂ receptors. Two of the compounds (11E and 11J) exhibited low micromolar CB₁ displacement with an IC₅₀ value of $\leq 2.0 \mu\text{M}$. Compounds 11A, 11B, 11E, 11H, and 11J showed significant displacement at the CB₂ receptor yielding binding affinities with an IC₅₀ value of $\leq 3.20 \mu\text{M}$. Two of the most promising compounds (11H and 11J) were further tested for functional activity and were found to be CB₂R agonists. The XP Glide docking did not produce any pose for 11H, which is in accordance with the experimental low binding affinity of 11H (29.45% displacement) toward the CB₁ receptor. MD simulations and binding free-energy calculations confirmed the stability of these compounds with CB₁ and CB₂ receptors. The MD study revealed that Ser173 and Ser285 are the two critical amino acids involved in the H-bonding interactions with these

analogues for CB₁ and CB₂ receptors. In future, by simply switching to (*R*)-citronellal as a chiral precursor, enantiomerically pure (–)-hexahydrocannabinoids could be achievable to develop novel analogues with better CB₁/CB₂ receptor isoform selectivities.

4. MATERIALS AND METHODS

4.1. Chemistry. All reactions were carried out under an argon atmosphere unless otherwise stated. Thin-layer chromatography was performed on precoated silica gel G and GP Uniplates. The plates were visualized with a 254 nm UV light, an iodine chamber, or charring with acid. Flash chromatography was carried out on silica gel 60 (particle size 32–63 μm , pore size 60 Å). ¹H NMR and ¹³C NMR spectra were recorded in CDCl₃ at 400 and 100 MHz or 500 and 125 MHz. The chemical shifts are reported in parts per million (ppm) downfield from

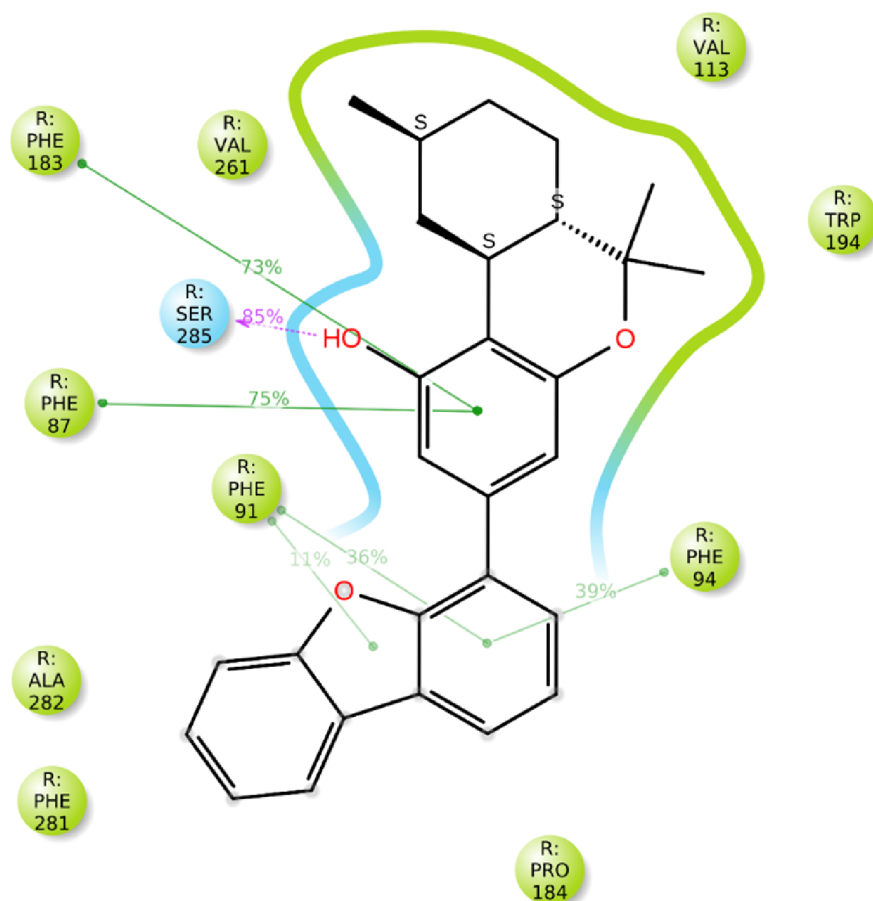


Figure 16. 2D diagram of atomic-level interaction of the CB₂-11H complex with key CB₂R residues during the 200 ns MD simulation.

tetramethylsilane, and *J* values are in Hz. The high-resolution mass spectra (HRMS) were recorded on a Waters Q-ToF of Micro mass spectrometer with an ESI lock spray source. Dry dichloromethane was prepared by distilling it over calcium hydride.

4.1.1. General Procedure for the Preparation of Compounds (11A–11N). To a solution of triflate **8** (80 mg, 0.18 mmol) in toluene/MeOH (9:1, v/v, 10 mL), boronic acid (0.27 mmol), 2 M aq Na₂CO₃ (100 μL), and tetrakis(triphenylphosphine)-palladium(0) (3 mg) were added and the reaction mixture was refluxed overnight. The reaction mixture was cooled, water was added, and the reaction mixture was extracted with ether. Combined organic layers were dried over MgSO₄, concentrated under vacuum, and purified by column chromatography using ethyl acetate in hexanes. The purified product was dissolved in 1% aq HCl in MeOH, heated to reflux, and stirred for 30 min. MeOH was evaporated, and the crude products were purified by column chromatography to afford compounds **11A–11N**. Triflate **8** was synthesized according to the procedure reported in our earlier work.¹⁶

(6a*S*,9*S*,10a*S*)-6,6,9-Trimethyl-3-phenyl-6a,7,8,9,10,10a-hexahydro-6*H*-benzo[*c*]chromen-1-ol (11A): [α]_D²⁵ = +137.0 (*c* 0.1, CHCl₃); ¹H NMR (CDCl₃, 500 MHz): δ 7.55 (d, *J* = 7.5 Hz, 2H), 7.41 (t, *J* = 7.5 Hz, 2H), 7.33 (t, *J* = 7.3 Hz, 1H), 6.71 (d, *J* = 1.5 Hz, 1H), 6.52 (d, *J* = 1.5 Hz, 1H), 4.93 (s, 1H), 3.11 (bd, *J* = 12.5 Hz, 1H), 2.56 (ddd, *J* = 2.5, 11.0, 13.5 Hz, 1H), 1.90 (m, 2H), 1.69 (m, 1H), 1.54 (t, *J* = 11.0 Hz, 1H), 1.44 (s, 3H), 1.17 (m, 2H), 1.14 (s, 3H), 1.0 (d, *J* = 6.5 Hz, 3H), 0.86 (dd, *J* = 11.5, 24.0, 1H). ¹³C NMR (CDCl₃, 125 MHz): δ 155.3, 155.0,

140.3, 140.2, 128.5(2C), 127.2, 126.7(2C), 112.2, 109.0, 106.1, 77.5, 49.4, 39.2, 35.8(2C), 33.2, 28.4, 28.1, 23.0, 19.5. HRMS (ESI⁺): calcd for C₂₂H₂₇O₂, 323.2011 (M + H)⁺, found 323.2008.

(6a*S*,9*S*,10a*S*)-3-(Benzo[*d*][1,3]dioxol-5-yl)-6,6,9-trimethyl-6a,7,8,9,10,10a-hexahydro-6*H*-benzo[*c*]chromen-1-ol (11B): [α]_D²⁵ = +92.0 (*c* 0.1, CHCl₃); ¹H NMR (CDCl₃, 500 MHz): δ 7.03 (s, 1H), 7.02 (d, *J* = 9.0 Hz, 1H), 6.85 (d, *J* = 9.0 Hz, 1H), 6.62 (d, *J* = 1.5 Hz, 1H), 6.43 (d, *J* = 1.4 Hz, 1H), 6.0 (s, 2H), 4.91 (bs, 1H), 3.09 (bd, *J* = 13.0 Hz, 1H), 2.54 (ddd, *J* = 2.5, 11.0, 13.5 Hz, 1H), 1.90 (m, 2H), 1.68 (m, 1H), 1.52 (t, *J* = 11.2 Hz, 1H), 1.43 (s, 3H), 1.16 (m, 2H), 1.13 (s, 3H), 0.98 (d, *J* = 6.5 Hz, 3H), 0.84 (dd, *J* = 12.0, 24.0, 1H); ¹³C NMR (CDCl₃, 125 MHz): δ 155.3, 155.0, 147.8, 146.8, 140.0, 134.7, 120.2, 111.9, 108.7, 108.4, 107.3, 105.9, 101.0, 77.5, 49.4, 39.2, 35.7(2C), 33.1, 28.3, 28.0, 22.9, 19.4. HRMS (ESI⁺): calcd for C₂₃H₂₇O₄, 367.1909 (M + H)⁺, found 367.1891.

4-((6a*S*,9*S*,10a*S*)-1-Hydroxy-6,6,9-trimethyl-6a,7,8,9,10,10a-hexahydro-6*H*-benzo[*c*]chromen-3-yl)-benzonitrile (11C): [α]_D²⁵ = +103.0 (*c* 0.1, CHCl₃); ¹H NMR (MeOH-*d*₄ + CDCl₃, 500 MHz): δ 7.70 (dd, *J* = 8.5, 11.5 Hz, 4H), 6.60 (d, *J* = 1.5 Hz, 1H), 6.56 (d, *J* = 1.6 Hz, 1H), 3.23 (bd, *J* = 13.0 Hz, 1H), 2.51 (ddd, *J* = 2.5, 11.5, 13.5 Hz, 1H), 1.87 (m, 2H), 1.66 (m, 1H), 1.47 (t, *J* = 10.5 Hz, 1H), 1.38 (s, 3H), 1.16 (m, 2H), 1.09 (s, 3H), 0.96 (d, *J* = 6.5 Hz, 3H), 0.7 (dd, *J* = 11.5, 24.0 Hz, 1H); ¹³C NMR (MeOH-*d*₄ + CDCl₃, 125 MHz): δ 157.0, 155.2, 145.5, 137.7, 132.1(2C), 127.1(2C), 118.7, 113.8, 110.0, 107.4, 105.6, 77.2, 49.5, 38.8, 36.0, 35.8, 33.1, 28.2, 27.4,

22.3, 18.7. HRMS (ESI⁺): calcd for C₂₃H₂₆NO₂, 348.1964 (M + H)⁺, found 348.1968.

(6aS,9S,10aS)-3-(Furan-3-yl)-6,6,9-trimethyl-6a,7,8,9,10,10a-hexahydro-6H-benzo[c]chromen-1-ol (11D): [α]_D²⁵ = +114.0 (c 0.1, CHCl₃); ¹H NMR (CDCl₃, 500 MHz): δ 7.65 (s, 1H), 7.44 (s, 1H), 6.62 (d, J = 1.4 Hz, 1H), 6.60 (d, J = 1.6 Hz, 1H), 6.41 (d, J = 1.5 Hz, 1H), 4.94 (s, 1H), 3.07 (bd, J = 13.0 Hz, 1H), 2.52 (ddd, J = 2.5, 11.5, 13.5 Hz, 1H), 1.89 (m, 2H), 1.67 (m, 1H), 1.51 (t, J = 11.0 Hz, 1H), 1.42 (s, 3H), 1.16 (m, 2H), 1.12 (s, 3H), 0.98 (d, J = 6.5 Hz, 3H), 0.84 (dd, J = 11.5, 24.0 Hz, 1H); ¹³C NMR (CDCl₃, 125 MHz): δ 155.3, 155.0, 143.3, 138.3, 131.5, 125.8, 112.1, 108.8, 107.8, 105.1, 77.5, 49.4, 39.2, 35.8, 33.2, 28.4, 28.1, 23.0, 19.4. HRMS (ESI⁺): calcd for C₂₀H₂₅O₃, 313.1804 (M + H)⁺, found 313.1819.

(6aS,9S,10aS)-6,6,9-Trimethyl-3-((E)-oct-1-en-1-yl)-6a,7,8,9,10,10a-hexahydro-6H-benzo[c]chromen-1-ol (11E): [α]_D²⁵ = +126.0 (c 0.1, CHCl₃); ¹H NMR (CDCl₃, 500 MHz): δ 6.45 (d, J = 1.5 Hz, 1H), 6.27 (d, J = 1.5 Hz, 1H), 6.15 (m, 2H), 4.86 (bs, 1H), 3.06 (bd, J = 12.5 Hz, 1H), 2.49 (ddd, J = 2.0, 10.5, 13.0 Hz, 1H), 2.18 (dd, J = 7.0, 14.0, 2H), 1.87 (m, 2H), 1.66 (m, 1H), 1.46 (m, 4H), 1.40 (s, 3H), 1.34 (m, 5H), 1.15 (m, 2H), 1.09 (s, 3H), 0.97 (d, J = 6.4 Hz, 3H), 0.92 (t, J = 6.5 Hz, 3H), 0.82 (dd, J = 12, 24 Hz, 1H); ¹³C NMR (CDCl₃, 125 MHz): δ 155.0, 154.8, 137.0, 131.0, 128.9, 111.9, 107.9, 105.1, 77.3, 49.4, 39.2, 35.9, 35.8, 33.2(2C), 32.1, 29.7, 29.2, 28.4, 28.1, 23.0, 19.4, 14.5. HRMS (ESI⁺): calcd for C₂₄H₃₇O₂, 357.2794 (M + H)⁺, found 357.2793.

(6aS,9S,10aS)-6,6,9-Trimethyl-3-((E)-4-(trifluoromethyl)styryl)-6a,7,8,9,10,10a-hexahydro-6H-benzo[c]chromen-1-ol (11F): [α]_D²⁵ = +106.0 (c 0.1, CHCl₃); ¹H NMR (CDCl₃, 500 MHz): δ 7.6 (d, J = 8.5 Hz, 2H), 7.55 (d, J = 8.5 Hz, 2H), 7.02 (dd, J = 6.5 Hz, 2H), 6.64 (d, J = 1.0 Hz, 1H), 6.45 (d, J = 1.5 Hz, 1H), 4.91 (s, 1H), 3.07 (bd, J = 13.0 Hz, 1H), 2.53 (ddd, J = 2.5, 11.0, 13.0 Hz, 1H), 1.9 (m, 2H), 1.68 (m, 1H), 1.52 (t, J = 11.0 Hz, 1H), 1.43 (s, 3H), 1.16 (m, 2H), 1.12 (s, 3H), 0.99 (d, J = 6.3 Hz, 3H), 0.83 (dd, J = 11.0, 23.0 Hz, 1H); ¹³C NMR (CDCl₃, 125 MHz): δ 155.3, 155.0, 140.6, 135.9, 130.5, 126.8, 126.4(4C), 125.5(2C), 113.7, 108.8, 105.8, 77.5, 49.3, 39.1, 36.0, 35.8, 33.2, 28.4, 28.0, 22.9, 19.4. HRMS (ESI⁺): calcd for C₂₅H₂₈O₂F₃, 417.2041 (M + H)⁺, found 417.2040.

(6aS,9S,10aS)-3-((E)-4-Chlorostyryl)-6,6,9-trimethyl-6a,7,8,9,10,10a-hexahydro-6H-benzo[c]chromen-1-ol (11G): [α]_D²⁵ = +112.0 (c 0.1, CHCl₃); ¹H NMR (CDCl₃, 500 MHz): δ 7.39 (d, J = 8.5 Hz, 2H), 7.32 (d, J = 8.5 Hz, 2H), 6.91 (dd, J = 16.0 Hz, 2H), 6.61 (d, J = 1.4 Hz, 1H), 6.42 (d, J = 1.5 Hz, 1H), 4.96 (s, 1H); 3.07 (bd, J = 12.5 Hz, 1H), 2.52 (ddd, J = 2.5, 11.0, 13.5 Hz, 1H), 1.89 (m, 2H), 1.67 (m, 1H), 1.51 (t, J = 11.0 Hz, 1H), 1.43 (s, 3H), 1.17 (m, 2H), 1.11 (s, 3H), 0.98 (d, J = 6.4 Hz, 3H), 0.82 (dd, J = 11.5, 24.0 Hz, 1H); ¹³C NMR (CDCl₃, 125 MHz): δ 155.2, 154.9, 136.3, 135.7, 132.9, 128.7(2C), 128.6, 127.5, 127.1(2C), 113.3, 108.6, 105.6, 77.5, 49.2, 39.1, 36.0, 35.9, 35.7, 33.2, 28.3, 28.0, 22.9, 19.4. HRMS (ESI⁺): calcd for C₂₄H₂₈O₂Cl, 383.1778 (M + H)⁺, found 383.1768.

(6aS,9S,10aS)-3-(Dibenzo[b,d]furan-4-yl)-6,6,9-trimethyl-6a,7,8,9,10,10a-hexahydro-6H-benzo[c]chromen-1-ol (11H): [α]_D²⁵ = +142.0 (c 0.1, CHCl₃); ¹H NMR (CDCl₃, 500 MHz): δ 7.98 (d, J = 7.5 Hz, 1H), 7.92 (dd, J = 1.0, 7.5 Hz, 1H), 7.60 (dd, J = 7.0, 8.0 Hz, 2H), 7.48 (dt, J = 1.0, 8.0 Hz, 1H), 7.38 (d, J = 7.5 Hz, 2H), 7.02 (d, J = 1.5 Hz, 1H), 6.94 (d, J = 1.6 Hz, 1H), 5.12 (s, 1H), 3.17 (bd, J = 13.0 Hz, 1H), 2.61 (ddd, J = 3.0,

11.5, 14.0 Hz, 1H), 1.91 (bd, 2H), 1.71 (m, 1H), 1.59 (t, J = 11.3 Hz, 1H), 1.47 (s, 3H), 1.17 (s, 3H), 1.15 (m, 2H), 1.01 (d, J = 6.7 Hz, 3H), 0.88 (dd, J = 11.5, 23.5 Hz, 1H); ¹³C NMR (CDCl₃, 125 MHz): δ 155.9, 155.3, 154.8, 153.0, 135.4, 127.1, 126.5, 125.1, 124.8, 124.1, 123.0, 122.6, 120.5, 119.5, 112.9, 111.9, 110.6, 107.9, 77.5, 49.4, 39.2, 36.0, 35.9, 33.3, 28.5, 28.2, 23.0, 19.5. HRMS (ESI⁺): calcd for C₂₈H₂₈O₃, 413.2038 (M + H)⁺, found 413.2105.

(6aS,9S,10aS)-6,6,9-Trimethyl-3-(4-phenoxyphenyl)-6a,7,8,9,10,10a-hexahydro-6H-benzo[c]chromen-1-ol (11I): [α]_D²⁵ = +75.0 (c 0.1, CHCl₃); ¹H NMR (CDCl₃, 500 MHz): δ 7.48 (d, J = 8.5 Hz, 2H), 7.38 (t, J = 8.0 Hz, 2H), 7.15 (t, J = 7.5 Hz, 1H), 7.07 (d, J = 8.0 Hz, 2H), 7.03 (d, J = 8.5 Hz, 2H), 6.89 (d, J = 1.5 Hz, 1H), 6.49 (d, J = 1.4 Hz, 1H), 5.33 (bs, 1H), 3.14 (bd, J = 13.0 Hz, 1H), 2.57 (ddd, J = 2.5, 11.0, 13.5 Hz, 1H), 1.90 (m, 2H), 1.69 (m, 1H), 1.55 (t, J = 11.3 Hz, 1H), 1.45 (s, 3H), 1.16 (m, 2H), 1.14 (s, 3H), 0.99 (d, J = 6.4 Hz, 3H), 0.85 (dd, J = 11.5, 23.5 Hz, 1H); ¹³C NMR (CDCl₃, 125 MHz): δ 156.9, 156.5, 155.3, 155.1, 139.6, 135.3, 129.7(2C), 127.9(2C), 123.3, 119.0(2C), 118.8(2C), 112.1, 108.6, 106.0, 77.6, 49.4, 39.2, 35.8(2C), 33.2, 28.4, 28.1, 23.0, 19.5. HRMS (ESI⁺): calcd for C₂₈H₃₁O₃, 415.2273 (M + H)⁺, found 415.2284.

(6aS,9S,10aS)-3-(Benzo[b]thiophen-3-yl)-6,6,9-trimethyl-6a,7,8,9,10,10a-hexahydro-6H-benzo[c]chromen-1-ol (11J): [α]_D²⁵ = +95.0 (c 0.1, CHCl₃); ¹H NMR (CDCl₃, 500 MHz): δ 8.0 (m, 1H); 7.91 (m, 1H); 7.37 (m, 2H); 7.33 (s, 1H); 6.72 (d, J = 1.4 Hz, 1H), 6.50 (d, J = 1.5 Hz, 1H), 5.37 (bs, 1H), 3.16 (bd, J = 13.0 Hz, 1H), 2.58 (ddd, J = 2.5, 11.0, 13.0 Hz, 1H), 1.91 (m, 2H), 1.70 (m, 1H), 1.57 (t, J = 11.3 Hz, 1H), 1.46 (s, 3H), 1.18 (m, 2H), 1.17 (s, 3H), 1.0 (d, J = 6.3 Hz, 3H), 0.86 (dd, J = 11.5, 23.5 Hz, 1H); ¹³C NMR (CDCl₃, 125 MHz): δ 155.2, 155.0, 140.5, 137.6, 137.3, 135.0, 124.3, 124.1, 123.2, 123.0, 122.8, 112.6, 110.5, 107.7, 77.6, 49.4, 39.1, 35.9(2C), 33.2, 28.4, 28.1, 23.0, 19.5. HRMS (ESI⁺): calcd for C₂₄H₂₇O₂S, 379.1732 (M + H)⁺, found 379.1735.

(6aS,9S,10aS)-3-(3,5-Bis(trifluoromethyl)phenyl)-6,6,9-trimethyl-6a,7,8,9,10,10a-hexahydro-6H-benzo[c]chromen-1-ol (11K): [α]_D²⁵ = +135.0 (c 0.1, CHCl₃); ¹H NMR (CDCl₃, 500 MHz): δ 7.98 (s, 2H), 7.83 (s, 1H), 6.72 (d, J = 1.6 Hz, 1H), 6.55 (d, J = 1.5 Hz, 1H), 5.40 (bs, 1H), 3.11 (bd, J = 13.0 Hz, 1H), 2.57 (ddd, J = 2.5, 11.0, 13.0 Hz, 1H), 1.91 (m, 2H), 1.69 (m, 1H), 1.54 (t, J = 11.0 Hz, 1H), 1.45 (s, 3H), 1.17 (m, 2H), 1.14 (s, 3H), 0.99 (d, J = 6.5 Hz, 3H), 0.86 (dd, J = 11.5, 24.0 Hz, 1H); ¹³C NMR (CDCl₃, 125 MHz): δ 155.7, 155.6, 142.4, 137.1, 131.9, 126.7, 124.4, 122.2, 120.7, 114.0, 109.0(2C), 105.9(2C), 77.8, 49.3, 39.0, 35.8, 35.7, 33.2, 28.4, 28.0, 22.9, 19.4. HRMS (ESI⁺): calcd for C₂₄H₂₅O₂F₆, 459.1759 (M + H)⁺, found 459.1739.

4-((6aS,9S,10aS)-1-Hydroxy-6,6,9-trimethyl-6a,7,8,9,10,10a-hexahydro-6H-benzo[c]chromen-3-yl)-N,N-dimethylbenzamide (11L): [α]_D²⁵ = +107.0 (c 0.1, CHCl₃); ¹H NMR (CDCl₃, 400 MHz): δ 7.39 (dd, J = 8, 17.2 Hz, 1H), 6.51 (d, J = 1.2 Hz, 1H), 6.19 (d, J = 1.6 Hz, 1H), 3.27 (br d, J = 13.2 Hz, 1H), 3.19 (s, 3H), 3.05 (s, 3H), 2.53 (ddd, J = 2.0, 10.8, 13.2 Hz, 1H), 1.88–1.84 (m, 2H), 1.68–1.67 (m, 1H), 1.48 (t, J = 11.2 Hz, 1H), 1.39 (s, 3H), 1.19–1.13 (m, 2H), 1.08 (s, 3H), 0.97 (d, J = 6.8 Hz, 3H), 0.77 (dd, J = 11.6, 23.6 Hz, 1H); ¹³C NMR (CDCl₃, 100 MHz): δ 172.35, 156.7, 155.2, 142.3, 138.6, 133.8, 127.2 (2C), 126.9(2C), 112.9, 107.5, 106.0, 77.2, 77.1, 49.2, 39.6, 38.6, 35.6, 32.9, 31.1, 28.1, 27.7, 22.6, 19.1; HRMS (ESI⁺): calcd for C₂₅H₃₂NO₃, 394.2382 (M + H)⁺, found 394.2375.

(6aS,9S,10aS)-6,6,9-Trimethyl-3-(pyridin-3-yl)-6a,7,8,9,10,10a-hexahydro-6H-benzo[c]chromen-1-ol (11M): $[\alpha]_D^{25} = +123.0$ (*c* 0.1, CHCl₃); ¹H NMR (CDCl₃, 400 MHz): δ 9.13 (d, *J* = 1.6 Hz, 1H), 8.6 (dd, *J* = 1.2, 4.8 Hz, 1H), 7.96 (dt, *J* = 1.6, 3.6, 8.0 Hz, 1H), 7.43 (dd, *J* = 4.8, 8.0 Hz, 1H), 6.87 (d, *J* = 1.6 Hz, 1H), 6.62 (d, *J* = 1.6 Hz, 1H), 3.37 (d, *J* = 12.8 Hz, 1H), 2.61 (ddd, *J* = 2.4, 11.2, 13.6 Hz, 1H), 1.91–1.89 (m, 2H), 1.75–1.73 (m, 1H), 1.55 (t, *J* = 11.2 Hz, 1H), 1.44 (s, 3H), 1.20–1.16 (m, 2H), 1.15 (s, 3H), 1.01 (d, *J* = 6.8 Hz, 3H), 0.83 (dd, *J* = 11.6, 24.0 Hz, 1H); ¹³C NMR (CDCl₃, 100 MHz): δ 157.4, 155.7, 146.8, 146.6, 137.4, 135.8, 135.1, 124.1, 113.9, 107.4, 106.3, 77.5, 49.4, 38.8, 36.1, 35.9, 33.2, 28.4, 28.1, 23.0, 19.5; HRMS (ESI⁺): calcd for C₂₁H₂₆NO₂, 324.1964 (M + H)⁺, found 324.1966.

(6aS,9S,10aS)-3-(4-(Dimethylamino)phenyl)-6,6,9-trimethyl-6a,7,8,9,10,10a-hexahydro-6H-benzo[c]chromen-1-ol (11N): $[\alpha]_D^{25} = +118.0$ (*c* 0.1, CHCl₃); ¹H NMR (CDCl₃, 500 MHz): δ 7.45 (d, *J* = 8.5 Hz, 2H), 6.78 (d, *J* = 8.5 Hz, 2H), 6.66 (d, *J* = 1.5 Hz, 1H), 6.46 (d, *J* = 1.5 Hz, 1H), 4.97 (s, 1H), 3.11 (br d, *J* = 12.5 Hz, 1H), 2.99 (s, 6H), 2.54 (ddd, *J* = 2.5, 11.0, 13.5 Hz, 1H), 1.91–1.88 (m, 2H), 1.7–1.68 (m, 1H), 1.53 (t, *J* = 11 Hz, 1H), 1.42 (s, 3H), 1.19–1.15 (m, 2H), 1.13 (s, 3H), 0.99 (d, *J* = 6.5 Hz, 3H), 0.85 (dd, *J* = 11.5, 24.0 Hz, 1H); ¹³C NMR (CDCl₃, 125 MHz): δ 155.2, 154.9, 149.4, 140.1, 134.6, 127.2(4C), 112.8, 107.9, 105.4, 77.2, 49.4, 40.9 (2C), 39.3, 35.9, 35.8, 33.2, 28.4, 28.1, 22.9, 19.5; HRMS (ESI⁺): calcd for C₂₄H₃₂NO₂, 366.2433 (M + H)⁺, found 366.2426.

(6aS,9S,10aS)-1-Hydroxy-6,6,9-trimethyl-6a,7,8,9,10,10a-hexahydro-6H-benzo[c]chromen-3-yl trifluoromethanesulfonate (7): ¹H NMR (CDCl₃, 500 MHz): δ 6.35 (d, 1H, *J* = 2.5 Hz); 6.25 (d, 1H, *J* = 2.5 Hz); 5.42 (bs, 1H); 3.00 (bd, 1H, *J* = 12.5 Hz); 2.46 (ddd, 1H, *J* = 2.5, 11.5, 14.0 Hz); 1.88 (m, 2H); 1.62 (m, 1H); 1.46 (m, 1H); 1.39 (s, 3H); 1.17 (m, 2H); 1.08 (s, 3H); 0.97 (d, 3H, *J* = 6.5 Hz); 0.78 (dd, 1H, *J* = 11.5, 24.5 Hz). ¹³C NMR (CDCl₃, 125 MHz): δ 156.0, 155.8, 120.3, 117.0, 113.5, 103.2, 100.6, 78.3, 49.5, 48.7, 38.4, 35.3, 32.8, 29.3, 27.9, 27.5, 22.5, 19.0. HRMS (ESI⁺): calcd for C₁₇H₂₂F₃O₅S, 395.1140 (M + H)⁺, found 395.1146.

4.2. Biological Evaluation. 4.2.1. Materials.

CP55,940 was purchased from Tocris (Bristol, U.K.), and BSA, Trizma hydrochloride, L-glutamine, penicillin, and streptomycin, non-enzymatic cell dissociation solution, and guanosine 50-diphosphate (GDP) were obtained from Sigma-Aldrich (St. Louis, MO, USA). G418 (geneticin) sulfate was purchased from Gibco (Paisley, U.K.). [³H]-CP55,940 was obtained from AP Biotech (Little Chalfont, U.K.) or PerkinElmer (Boston, MA, USA), and [³⁵S]-GTP γ S was obtained from PerkinElmer (Boston, MA, USA). GTP γ S adenosine deaminase and hygromycin B were obtained from Roche Diagnostic (Indianapolis, IN, USA). Expression clones containing CB₁R and CB₂R full-length cDNA were purchased OriGene (Rockville, MD, USA).

4.2.2. Cell Lines and Culture. Human embryonic kidney (HEK) 293 cells were purchased from the American Type Culture Collection. The cells were grown in 150 cm² Corning cell culture dishes with Dulbecco's modified Eagle's medium/Ham's F12 medium supplemented with 10% fetal bovine serum (FBS), 2 mM glutamine, penicillin (100 U/mL), and streptomycin (100 μ g/mL) in an atmosphere of 5% CO₂.

4.2.3. Transfection and Stable Expression of CB₁ and CB₂ Receptors in Mammalian Cell Lines. HEK293 cells were collected and transiently transfected with the human CB₁ and CB₂ receptors. cDNA containing expression clones were used to

generate separate cell lines expressing either the CB₁ or the CB₂ receptors (50 μ g/mL) using electroporation (70 ms, single pulse, 150 V). The transfected cells were grown in a 150 cm² cell culture Petri dish. For selection, G418 antibiotic solution (800 μ g/mL) was used. After selection, the HEK293 cells were further cultured until single colonies were obtained. The colonies with a binding ratio (%) over 50% were chosen for binding and functional assays.

4.2.4. Cell Membrane Preparation. Cell plasma membranes were prepared from HEK293 cells with stable expression of CB₁ and CB₂ receptors. Cells grown to confluency were collected by scraping and spun at 2000g for 10 min at 4 °C. Crude membranes were prepared by homogenization of the cells in 50 mM Tris-HCl (pH 7.5) and centrifugation at 1000g for 5 min. The supernatant was centrifuged at 40,000g for 40 min at 4 °C, and the pellet was resuspended in a buffer consisting of 50 mM Tris-HCl (pH 7.5), 5 mM MgCl₂, and 1 mM EDTA and stored at –80 °C until use.

4.2.5. Competitive Receptor Binding Assay. Competitive binding assays were performed with a recently modified rapid filtration assay referred to the methods described earlier.^{17,22,23} Briefly, cell membranes (5 μ g of CB₁R or 1 μ g of CB₂R) were incubated with 1.079 nM [³H]-CP55,940 (CB₁R) or 1.002 nM [³H]-CP55,940 (CB₂R) and test compounds in 50 mM Tris-EDTA buffer (50 mM Tris, pH 7.4, 20 mM disodium EDTA, 154 mM NaCl, and 0.2% bovine serum albumin) for 1.5 h at 37 °C with gentle shaking (total volume 200 μ L). The reaction was terminated by rapid vacuum filtration onto a PerkinElmer Unifilter GF/C-96 filter plate and washed 10 times with ice-cold 50 mM Tris-EDTA containing 0.2% BSA (pH 7.4); bound radioactivity was quantified by the Packard TopCount Scintillation Counter. Specific binding was defined as the difference between the binding that occurred in the presence and the absence of 1 μ M unlabeled CP55,940. All of the experimental data (IC₅₀, K_i, and EC₅₀) were analyzed using a nonlinear regression curve fit model using GraphPad Prism 9.1 software (GraphPad Software, Inc., San Diego, CA, USA), and the K_d value was calculated. Each compound was tested in triplicate unless stated otherwise.

4.2.6. GTP γ S Binding Assay. The method for measuring agonist-stimulated [³⁵S]-GTP γ S binding to the human CB₁ and CB₂ receptors was used as described previously.²⁴ In brief, binding reactions were carried out in 96-well microplates in a final volume of 500 μ L. Cell membranes (20 μ g) were incubated with 0.5 nM [³⁵S]-GTP γ S, 30 μ M GDP, and compounds in assay buffer (50 mM Tris-HCl, 150 mM NaCl, 9 mM MgCl₂, 0.2 mM EGTA, and 1.4 mg/mL BSA, pH 7.4) for 2 h at 37 °C with gentle shaking. The nonspecific binding (NSB) was determined using 40 mM nonradiolabeled guanosine 5'-(γ -thio) triphosphate (GTP γ S) (PerkinElmer, Waltham, MA). The positive control was attained by utilizing 10 μ M unlabeled CP55,940 for the test compound. The reaction was terminated by rapid vacuum filtration, and the membranes were harvested onto a PerkinElmer Unifilter GF/B-96 filter plate and washed three times with ice-cold washing buffer (10 mM Tris-HCl, pH 7.4), and the bound radioactivity was quantified by a Packard TopCount Scintillation Counter.

4.3. Computational Methods. 4.3.1. Protein Preparation and Receptor Grid Generation. The X-ray crystal structure of cannabinoid receptors 1 (PDB ID: 5XRA)²⁵ and the Cryo-EM structure of CB₂ (PDB ID: 6PT0)²⁶ were downloaded from the RCSB Protein Data Bank (PDB). These structures were prepared by adding hydrogen atoms, bond orders, and missing

side chains and by proper ionization at physiological pH 7.4 using the Protein Preparation wizard module implemented in the Schrödinger software.

4.3.2. Ligand Preparation. The 2D structures of **11E**, **11H**, and **11J** were drawn using the 2D-Sketcher module implemented in the Schrödinger software²⁷ and prepared using the LigPrep²⁸ module of the Schrödinger software,²⁷ using the OPLS3e force field²⁹ and a pH range of 7.0 ± 2.0 using Epik.³⁰

4.3.3. Ligand Docking within the Orthosteric Binding Site. The centroid of the orthosteric ligand co-crystallized with CB₁R (PDB ID: 5XRA), and CB₂R (PDB ID: 6PT0) were used to define the center of the receptor grid for docking. XP docking (Glide, Schrödinger) was used with flexible ligand sampling, keeping the receptor rigid.^{31,32} The best-docked pose of the ligand was selected based on the Glide Emodel scores.

4.3.4. MD Simulations for CB₁-11J, CB₂-11J, and CB₂-11H Complexes. MD simulations were performed to further assess the stabilities and interaction profiles of the best complexes of CB₁-11J, CB₂-11J, and CB₂-11H obtained after the docking study. A similar MD simulation protocol was applied to that described previously.^{33,34} In brief, the complex was embedded in a POPC (1-palmitoyl-2-oleoyl-*sn*-glycero-3-phosphocholine) bilayer and solvated with 11 Å TIP3P water buffer using the OPLS3e (optimized potentials for liquid simulations 3) force field in Desmond,³⁵ Schrödinger. The system was neutralized, and 0.15 M NaCl was added to the system. The system was equilibrated using the following protocol. First, the system was simulated for 100 ps using Brownian dynamics in the NVT ensemble at 10 K with the restraint of 50 kcal/mol on solute heavy atoms. Second, a 500 ps simulation was run in the NVT ensemble using the Berendsen thermostat (10 K) while retaining the restraint on solute heavy atoms. Third, a 300 ps simulation was run in the NPT ensemble using the Berendsen thermostat (10 K) and barostat (1 atm) while restraints were retained. The system was gradually heated to 300 K over the next 500 ps. A final 500 ps simulation was performed in which all restraints were removed before the production run. The final production run (200 ns) was performed in the NPT ensemble using a timestep of 2 fs. The Langevin thermostat and Langevin were used for the production runs.

■ ASSOCIATED CONTENT

SI Supporting Information

The Supporting Information is available free of charge at <https://pubs.acs.org/doi/10.1021/acsomega.1c02413>.

3D overlaid representation of **11H**, **11J**, and Δ^9 -THC against the CB₂ receptor; RMSF plots for **11J** and **11H**; NMR and HR-MS spectral data for compounds **11A**–**11K** (PDF)

■ AUTHOR INFORMATION

Corresponding Author

Amar G. Chittiboyina – National Center for Natural Products Research, University of Mississippi, University, Mississippi 38677, United States; orcid.org/0000-0002-7047-5373; Phone: +1-662-915-1572; Email: amar@olemiss.edu; Fax: +1-662-915-7989

Authors

Saqain Haider – National Center for Natural Products Research, University of Mississippi, University, Mississippi 38677, United States; orcid.org/0000-0002-1738-6945

Pankaj Pandey – National Center for Natural Products Research, University of Mississippi, University, Mississippi 38677, United States; orcid.org/0000-0001-9128-8254

Chada Raji Reddy – Department of Organic Synthesis and Process Chemistry, CSIR-Indian Institute of Chemical Technology, Hyderabad 500007, India; orcid.org/0000-0003-1491-7381

Janet A. Lambert – Department of Pharmacology, School of Medicine, University of Nevada, Reno, Nevada 89557, United States

Complete contact information is available at:

<https://pubs.acs.org/10.1021/acsomega.1c02413>

Notes

The authors declare no competing financial interest.

■ ACKNOWLEDGMENTS

This research is in part supported by “Discovery & Development of Natural Products for Pharmaceutical & Agrichemical Applications” funded by the United States Department of Agriculture, Agricultural Research Service, Specific Cooperative Agreement No. 58-6060-6-015.

■ REFERENCES

- (1) Hanuš, L. O.; Meyer, S. M.; Muñoz, E.; Tagliatela-Scafati, O.; Appendino, G. Phytocannabinoids: A unified critical inventory. *Nat. Prod. Rep.* **2016**, *33*, 1357–1392.
- (2) Kendall, D. A.; Yudowski, G. A. Cannabinoid Receptors in the Central Nervous System: Their Signaling and Roles in Disease. *Front. Cell. Neurosci.* **2017**, *10*, 1–10.
- (3) Calignano, A.; La Rana, G.; Giuffrida, A.; Piomelli, D. Control of pain initiation by endogenous cannabinoids. *Nature* **1998**, *394*, 277–281.
- (4) Sagredo, O.; Ramos, J. A.; Decio, A.; Mechoulam, R.; Fernández-Ruiz, J. Cannabidiol reduced the striatal atrophy caused 3-nitropropionic acid in vivo by mechanisms independent of the activation of cannabinoid, vanilloid TRPV1 and adenosine A2A receptors. *Eur. J. Neurosci.* **2007**, *26*, 843–851.
- (5) Shoemaker, J. L.; Seely, K. A.; Reed, R. L.; Crow, J. P.; Prather, P. L. The CB2 cannabinoid agonist AM-1241 prolongs survival in a transgenic mouse model of amyotrophic lateral sclerosis when initiated at symptom onset. *J. Neurochem.* **2007**, *101*, 87–98.
- (6) Netherland, C. D.; Pickle, T. G.; Bales, A.; Thewke, D. P. Cannabinoid receptor type 2 (CB2) deficiency alters atherosclerotic lesion formation in hyperlipidemic Ldlr-null mice. *Atherosclerosis* **2010**, *213*, 102–108.
- (7) Barutta, F.; Piscitelli, F.; Pinach, S.; Bruno, G.; Gambino, R.; Rastaldi, M. P.; Salvidio, G.; Di Marzo, V.; Cavallo Perin, P.; Gruden, G. Protective role of cannabinoid receptor type 2 in a mouse model of diabetic nephropathy. *Diabetes* **2011**, *60*, 2386–2396.
- (8) Alswat, K. A. The role of endocannabinoids system in fatty liver disease and therapeutic potentials. *Saudi J. Gastroenterol.* **2013**, *19*, 144–151.
- (9) Slater, S.; Lasonkar, P. B.; Haider, S.; Alqahatani, M. J.; Chittiboyina, A. G.; Khan, I. A. One-step, stereoselective synthesis of octahydrochromanes via the Prins reaction and their cannabinoid activities. *Tetrahedron Lett.* **2018**, *59*, 807–810.
- (10) Pacher, P.; Bátkai, S.; Kunos, G. The endocannabinoid system as an emerging target of pharmacotherapy. *Pharmacol. Rev.* **2006**, *58*, 389–462.
- (11) Pertwee, R. G. The diverse CB₁ and CB₂ receptor pharmacology of three plant cannabinoids: Delta9-tetrahydrocannabinol, cannabidiol

- and delta9-tetrahydrocannabinol. *Br. J. Pharmacol.* **2008**, *153*, 199–215.
- (12) Calapai, F.; Cardia, L.; Sorbara, E. E.; Navarra, M.; Gangemi, S.; Calapai, G.; Mannucci, C. Cannabinoids, Blood-Brain Barrier, and Brain Disposition. *Pharmaceutics* **2020**, *12*, 265.
- (13) Laprairie, R. B.; Bagher, A. M.; Kelly, M. E.; Denovan-Wright, E. M. Cannabidiol is a negative allosteric modulator of the cannabinoid CB₁ receptor. *Br. J. Pharmacol.* **2015**, *172*, 4790–4805.
- (14) House, A.; Pitch, B. AMA Meeting: Delegates Support Review of Marijuana's Schedule I Status, 2009.
- (15) Muhammad, I.; Li, X.-C.; Dunbar, D. C.; ElSohly, M. A.; Khan, I. A. Antimalarial (+)-trans-hexahydrodibenzopyran derivatives from *Machaerium multiflorum*. *J. Nat. Prod.* **2001**, *64*, 1322–1325.
- (16) Chittiboyina, A. G.; Reddy, C. R.; Watkins, E. B.; Avery, M. A. First synthesis of antimalarial Machaeriols A and B. *Tetrahedron Lett.* **2004**, *45*, 1689–1691.
- (17) Pandey, P.; Roy, K. K.; Liu, H.; Ma, G.; Pettaway, S.; Alsharif, W. F.; Gadepalli, R. S.; Rimoldi, J. M.; McCurdy, C. R.; Cutler, S. J.; Doerksen, R. J. Structure-based identification of potent natural product chemotypes as cannabinoid receptor 1 inverse agonists. *Molecules* **2018**, *23*, 2630.
- (18) Ramírez, D.; Caballero, J. Is It Reliable to Take the Molecular Docking Top Scoring Position as the Best Solution without Considering Available Structural Data? *Molecules* **2018**, *23*, 1038.
- (19) Miszta, P.; Pasznik, P.; Jakowiecki, J.; Sztylek, A.; Latek, D.; Filipek, S. GPCRm: A homology modeling web service with triple membrane-fitted quality assessment of GPCR models. *Nucleic Acids Res.* **2018**, *46*, W387–W395.
- (20) Rhee, M. H. Functional role of serine residues of transmembrane dopamin VII in signal transduction of CB₂ cannabinoid receptor. *J. Vet. Sci.* **2002**, *3*, 185–192.
- (21) Alonso, H.; Bliznyuk, A. A.; Gready, J. E. Combining docking and molecular dynamic simulations in drug design. *Med. Res. Rev.* **2006**, *26*, 531–568.
- (22) Ma, G.; Bavadekar, S. A.; Davis, Y. M.; Lalchandani, S. G.; Nagmani, R.; Schaneberg, B. T.; Khan, I. A.; Feller, D. R. Pharmacological effects of ephedrine alkaloids on human α 1- and α 2-adrenergic receptor subtypes. *J. Pharmacol. Exp. Ther.* **2007**, *322*, 214–221.
- (23) Felder, C. C.; Veluz, J. S.; Williams, H. L.; Briley, E. M.; Matsuda, L. A. Cannabinoid agonists stimulate both receptor- and non-receptor-mediated signal transduction pathways in cells transfected with and expressing cannabinoid receptor clones. *Mol. Pharmacol.* **1992**, *42*, 838–845.
- (24) Xiong, W.; Cheng, K.; Cui, T.; Godlewski, G.; Rice, K. C.; Xu, Y.; Zhang, L. Cannabinoid potentiation of glycine receptors contributes to cannabis-induced analgesia. *Nat. Chem. Biol.* **2011**, *7*, 296–303.
- (25) Hua, T.; Vemuri, K.; Nikas, S. P.; Laprairie, R. B.; Wu, Y.; Qu, L.; Pu, M.; Korde, A.; Jiang, S.; Ho, J.-H. Crystal structures of agonist-bound human cannabinoid receptor CB₁. *Nature* **2017**, *547*, 468–471.
- (26) Xing, C.; Zhuang, Y.; Xu, T.-H.; Feng, Z.; Zhou, X. E.; Chen, M.; Wang, L.; Meng, X.; Xue, Y.; Wang, J. Cryo-EM structure of the human cannabinoid receptor CB₂-Gi signaling complex. *Cell* **2020**, *180*, e13.
- (27) Schrödinger Release 2020-4: Maestro version 12.6.144; Schrödinger, LLC: New York, NY, 2020.
- (28) Schrödinger Release 2020-4: LigPrep; Schrödinger, LLC: New York, NY, 2020.
- (29) Roos, K.; Wu, C.; Damm, W.; Reboul, M.; Stevenson, J. M.; Lu, C.; Dahlgren, M. K.; Mondal, S.; Chen, W.; Wang, L.; Abel, R.; Friesner, R. A.; Harder, E. D. OPLS3e: Extending Force Field Coverage for Drug-Like Small Molecules. *J. Chem. Theory Comput.* **2019**, *15*, 1863–1874.
- (30) Shelley, J. C.; Cholleti, A.; Frye, L. L.; Greenwood, J. R.; Timlin, M. R.; Uchimaya, M. Epik: A software program for pK_a prediction and protonation state generation for drug-like molecules. *J. Comput.-Aided Mol. Des.* **2007**, *21*, 681–691.
- (31) Friesner, R. A.; Banks, J. L.; Murphy, R. B.; Halgren, T. A.; Klicic, J. J.; Mainz, D. T.; Repasky, M. P.; Knoll, E. H.; Shelley, M.; Perry, J. K. Glide: A new approach for rapid, accurate docking and scoring. 1. Method and assessment of docking accuracy. *J. Med. Chem.* **2004**, *47*, 1739–1749.
- (32) Schrödinger Release 2020-4: Glide; Schrödinger, LLC: New York, NY, 2020.
- (33) Pandey, P.; Chatterjee, S.; Berida, T.; Doerksen, R. J.; Roy, S. Identification of potential non-nucleoside MraY inhibitors for tuberculosis chemotherapy using structure-based virtual screening. *J. Biomol. Struct. Dyn.* **2020**, DOI: 10.1080/07391102.2020.1862705.
- (34) Stoddard, S. V.; Stoddard, S. D.; Oelkers, B. K.; Fitts, K.; Whalum, K.; Whalum, K.; Hemphill, A. D.; Manikonda, J.; Martinez, L. M.; Riley, E. G.; Roof, C. M.; Sarwar, N.; Thomas, D. M.; Ulmer, E.; Wallace, F. E.; Pandey, P.; Roy, S. Optimization rules for SARS-CoV-2 Mpro antivirals: Ensemble docking and exploration of the coronavirus protease active site. *Viruses* **2020**, *12*, 942.
- (35) D.E. Shaw Research. *Shaw Research Desmond Molecular Dynamics System; Maestro-Desmond Interoperability Tools*; Schrödinger, LLC: New York, NY, USA, 2019.